Computational Studies on Polymer Adhesion at the Surface of γ-Al_2O_3. I. The Adsorption of Adhesive Component Molecules from the Gas Phase

Jan M. Knaup,*,†,‡ Christof Köhler,†,‡ Thomas Frauenheim,†,‡ Alexander T. Blumenau,§ Marc Amkreutz,⊥ Peter Schiffels,⊥ Bernhard Schneider,⊥ and Otto-Diedrich Hennemann⊥

Bremen Center for Computational Materials Science, University of Bremen, Otto-Hahn-Allee 1, 28359 Bremen, Germany, Theoretical Physics, Faculty of Science, Universität Paderborn, 33095 Paderborn, Germany, Max-Planck-Institut für Eisenforschung GmbH, Max-Planck-Strasse 1, 40237 Düsseldorf, Germany, and Fraunhofer-Institut für Fertigungstechnik und Angewandte Materialforschung, Wiener Strasse 12, 28359 Bremen, Germany

Received: June 19, 2006; In Final Form: August 2, 2006

Ⓦ This paper contains enhanced objects available on the Internet at http://pubs.acs.org/jpcbfk.

We calculate the minimum energy paths and reaction energies of the adsorption of the epoxide adhesive components diglycidylesterbisphenol A (DGEBA), diethyltriamine (DETA), and the adhesion promoter 3-aminopropylmethoxysilane (AMEO) at two different sites on a model of the native Al_2O_3 surface, using the nudged elastic band algorithm in conjunction with self-consistent charge−density functional based tight binding. Our results show that the chosen combination of methods is well suited to obtain an overview of the reaction mechanisms and kinetics of the adsorption of organic molecules on inorganic surfaces. The obtained MEP-s show that there is preference for the adsorption of the adhesion promoter, AMEO, over the resin, DGEBA, while the adsorption of the curing agent, DETA, is unfavorable. Our approach also gives an insight into the ranges of the mechanical and electronic influences of the adsorption process on the interface, which neither full ab initio methods nor force field approaches can provide. These results will help to develop a quantum mechanics-molecular mechanics multiscale embedding scheme for more detailed studies of organic/inorganic hybrid interface reactions.

I. Introduction

During the past two decades aluminum has constantly gained importance in technical applications, with its use spreading from aerospace to automotive applications and now covering nearly every area of industrial and consumer appliances. Nowadays, adhesive technology has achieved advances which enable adhesive bonding of metal parts to supplement or even replace traditional metal joining technologies such as welding, bolting, or riveting. Related to this is development of metal−resin or metal−resin−fiber compound materials, which have recently advanced to the point of technical application.[1] The demands for lighter and at the same time stronger materials, to build more fuel-efficient, i.e., lighter, vehicles and aircraft without sacrificing structural strength leads to a strong interest in the development and improvement of fiber reinforced aluminum−polymer hybrid materials and adhesive bonding technology for aluminum. For both of these technologies, the aluminum−polymer adhesion is of crucial importance.

Since, outside high-vacuum environments, aluminum instantly develops a surface oxide layer,[2,3] the problem of adhesion on aluminum translates into the problem of adhesion on native aluminum oxide. The improvement of adhesion technology requires an understanding of the underlying chemical processes of the bonding of organic adhesives to the alumina surface. In this study we aim at finding a suitable methodology for gaining insight into the initial bonding of adhesive component molecules as well as the bonding competition between different organic species at the native Al_2O_3 surface. To achieve this, we concentrate on a model adhesive system, comprising diglycidylesterbisphenol A (DGEBA) as the resin, diethyltriamine (DETA) as the curing agent, and 3-aminopropylmethoxysilane (sold as Dynasilan AMEO, here referred to as AMEO) as an adhesion promoter component. Although our results are focused on an adhesive, some of the examined components are also used in compound materials or paints, and our method is sufficiently general to be transferable to the adsorption of any organic molecule of similar size on inorganic surfaces.

Native alumina, created by corrosion of Al in air, is usually described as γ-Al_2O_3, which is formed by a pseudoamorphous defective spinel structure in which Al atoms and vacancies are randomly distributed among the tetrahedral and octahedral sites within a perfect fcc sublattice of oxygen atoms.[4−9] However, there is still controversy in the literature concerning the crystallography of γ-alumina. A recent extensive study, combining experimental and theoretical approaches, suggests that the description of γ-alumina requires a significant number of Al atoms on nonspinel positions to be accurate.[10] Extensive review of the literature concerned with the bulk structure of γ-alumina is given in refs 11 and 12. As the underlying bulk structure is amorphous, the surface does not exhibit any regular reconstruction. The main characteristics of the surface are the distribution statistics and density of surface Al on tetrahedral and octahedral sites as well as on the distribution of hydroxyl groups at the surface. A mesoscopic model of the (100) surface of spinel-like γ-alumina and its hydroxylation has already been presented in ref 13.

It is well-known that in a moist environment, such as air, the Al_2O_3 surface quickly absorbs water, both molecularly and

* knaup@bccms.uni-bremen.de
† University of Bremen.
‡ Universität Paderborn.
§ Max-Planck-Institut für Eisenforschung GmbH.
⊥ Fraunhofer-Institut für Fertigungstechnik und Angewandte Materialforschung.

10.1021/jp063814w CCC: $33.50
Published on Web 09/15/2006

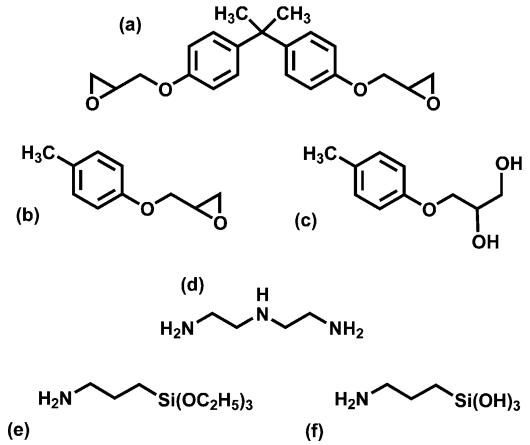

Figure 1. The examined molecules (a) DGEBA, (b) t-DGEBA, (c) t-DGEBA$^{(open)}$, (d) DETA, (e) AMEO, and (f) AMEO$^{(hyd)}$.

dissociatively.[13−16] It is therefore essential to include the hydroxylation of the surface in any study of its chemistry. Since alumina in general and especially γ-alumina is of high interest as a catalyst for the chemical industry, a large number of studies on the surface reactivity have been performed, most of which are concerned with the surface acidity. Reviewing this extensive literature is beyond the scope of this work. An extensive overview can be found in refs 9 and 17 and references therein. Investigations on the adsorption of methanol at the hydroxylated surface show that these react with hydroxyl groups attached to surface aluminums by condensation.[18,19] A study of the adsorption of maleic acid anhydride[20] and theoretical investigations[21] on the adsorption of adhesive components on amorphous SiO_2 and hydroxylated α-Al_2O_3 also find condensation reactions on the alumina surface, except for DGEBA, which is found to react with the surface by additive ring opening. We therefore assume that similar reactions will occur in the system studied here; however, we assume the ring opening of DGEBA to occur in the liquid phase of the adhesive mixture, independent of the surface. Therefore we examine the ring opening of DGEBA by water and the condensation reaction of the opened DGEBA separately.

In a recent study of the DETA absorption energetics[22] reaction energies of $\sim$35 kcal mol^{-1} have been observed for a chemisorption at an octahedral surface aluminum site. In this study we concentrate on the interaction of the adhesive components with surface hydroxyl groups, which results in a condensation reaction for the adsorption of DETA.

As DGEBA has a mirror plane, we consider a truncated molecule that only contains one phenol-ring and one epoxy group, referred to as t-DGEBA (cf. Figure 1a,b). Since AMEO can be expected to rapidly lose its ethyl groups and hydrolyze in an aqueous solution, we only study the interaction of the hydrolyzed form of AMEO, which we refer to as AMEO$^{(hyd)}$ (cf. Figure 1e,f). In our model, the adsorption of DGEBA depends on the prior opening and hydroxylation of at least one oxirane ring. This catalyzed reaction is not limited to the alumina surface but must happen throughout the adhesive mixture, the ring-opened, truncated DGEBA molecule will henceforth be referred to as t-DGEBA$^{(open)}$ (cf. Figure 1c). After these considerations, we examine the following reactions at the surface:

$$\text{t-DGEBA}^{(open)} + \text{surf.} \xrightarrow{\Delta E} (\text{t-DGEBA} + \text{surf.}) + H_2O \quad (1)$$

$$\text{DETA} + \text{surf.} \xrightarrow{\Delta E} (\text{DETA} + \text{surf.}) + H_2O \quad (2)$$

$$\text{AMEO}^{(hyd)} + \text{surf.} \xrightarrow{\Delta E} (\text{AMEO}^{(hyd)} + \text{surf.}) + H_2O \quad (3)$$

where surf. denotes the hydroxylated surface model and (species + surf.) denotes the structure of the organic species adsorbed at the surface. Additionally, we also consider the reaction

$$\text{t-DGEBA} + 2H_2O \xrightarrow{\Delta E} \text{t-DGEBA}^{(open)} + H_2O \quad (4)$$

Here, the second water molecule stabilizes the ring opening.

II. Methods

A detailed insight into the adsorption competition of different species on a surface requires accurate knowledge about the distribution of adsorption sites on the surface as well as accurate kinetic constants for all combinations of organic molecule and surface site. Here we calculate the minimum energy paths (MEP-s) of the adsorption reactions on selected surface sites as a first step in that direction. Although the MEP-s lack the inclusion of entropy effects, the calculation of the latter, purely with ab initio or *tight-binding* approaches, is far too computationally expensive. Multiscale methods could solve this problem, but before they can be applied, it is necessary to obtain at least an overview of the interactions and influence areas in the given system. Only then can a suitable method, which includes the relevant effects, and a QM cluster of suitable size for QM-MM coupling be chosen.

A. DFTB. On the basis of these considerations, we choose to constrain ourselves to a search of the MEP using *self-consistent charge−density functional based tight-binding* (SCC-DFTB)[23] for the energies and forces calculations. We iterate the SCC until between two subsequent steps either the maximum Mulliken charge difference is below 10^{-4} e$^-$ or the total energy difference is below 10^{-8} Ha.

The parameter sets (Slater−Koster files) we use in this study have been validated elsewhere for this system[24] except for the Al−O interaction. Our results for bulk Al_2O_3, shown in Table 1 and discussed in section 3, show that our parametrization of Al−O produces results in good accordance to the available experimental data. Additionally, we calculate the total energies of the DFTB-relaxed bulk alumina structures using density functional theory (DFT) in the local density approximation (LDA) as provided by the SIESTA 2.0[25] code. In these calculations we use a *double-*ζ basis including polarization functions, comparable to a 21G* basis with the cutoff radius determined by a maximum energy shift, due to the confinement of the first ζ shell, of 0.02 Ry, and Troulier−Martins[26] pseudopotentials. We set the mesh cutoff to 90 Ry. We solve the Kohn−Sham equations by matrix diagonalization rather than the order-*N* method provided by SIESTA. The LDA results, listed in Table 1, agree very well with our DFTB results in terms of energy differences between the different crystal structures.

B. Reaction Energies. We estimate the reaction energies for the adsorption reactions using the total energies of the relaxed, isolated educts and products. This choice neglects the effects of a possible physisorption of secondary products, i.e., water molecules, at the alumina surface. We choose this approach for the following reasons: The alumina surface is already covered with water under real conditions. Applying the polymer to the surface will lead to a solution of this water in the polymer, but since simulations show that physisorbed water on hydroxylated alumina forms complexes with the surface and other water molecules with an energy gain of at least 20 kcal/mol or more, it is most unlikely that these physisorbed water molecules will

TABLE 1: SCC-DFTB and LDA Results on γ-Al_2O_3[a]

structure	N_{cell}	E_{tot}^{DFTB} [eV/Al_2O_3]	E_{tot}^{LDA} [eV/Al_2O_3]	ρ [g cm^{-3}]	Al−O [Å]
hausmannite	80	−334.98	−1425.70	3.65	1.88(0.07)
spinel cub. 1	160	−335.41	−1426.36	3.66	1.88(0.07)
spinel cub. 2	160	−335.41	−1426.36	3.66	1.88(0.07)
spinel cub. 3	160	−335.39	−1426.37	3.64	1.88(0.06)
spinel rhomb.	80	−335.05	−1425.74	3.66	1.88(0.06)

[a] N_{cell} is the number of atoms per unit cell, Al−O is the mean Al−O bond length and its statistical error.

be soluted during polymer application. Hence, a physisorption of the water, formed during the reaction, is not expected since the relevant sites are still occupied. However, a hydrogen bridge bonding may occur, resulting in an energy gain of approximately 5−10 kcal/mol in this case, which is small compared to the reaction energies and can be expected to be similar for all examined reactions. On the other hand, effects such as the solvation energy of the water built during the reaction in the polymer and water covering the surface or entropic effects are computationally too costly to be considered.

We follow the convention, to include the reaction energy on the right-hand side of the reaction equation, i.e., a negative reaction energy denotes an exothermic reaction. We use conjugate gradients (CG) relaxation to minimize the total energies until the forces are below 10^{-4} au.

C. Nudged Elastic Band. We employ the *nudged elastic band*[27] (NEB) method to obtain a sampling of the total energies along the examined reaction paths. To this end, NEB works with a chain of intermediate geometries, called images, along the reaction route. These images are connected by virtual springs, which distribute the images along the reaction coordinate and keep the images from traveling down the potential energy hypersurface into local minima. NEB differs from other chain-of-states methods in that only spring force constants parallel to the local tangents at the images are regarded, while neglecting tangential components of the calculated atomic forces. The chain of images is then optimized to minimize the NEB force for all intermediate images along the path, while the start and end geometries are kept fixed. During the minimization, the magnitude of the tangential force component, i.e., the virtual spring forces, indicates the convergence with respect to the even-spaced distribution of the images along the reaction path, while the orthogonal force is correlated to the deviation of the images from the valley of the potential energy hypersurface.

NEB yields a sampling of the total energies along the path, but in general does not produce an image that directly corresponds to the saddle point. Therefore an interpolation of the total energies is necessary. This interpolation is most frequently performed by a cubic spline fit of the image energies, with the gradients at the start and end images set to zero. Another approach is to fit a cubic polynomial to each segment connecting two images, using the tangential *real force* (i.e., DFTB-calculated force) components to determine the energy gradient at each image.[28]

The NEB formalism has already been used in surface science for many different applications (e.g. in refs 29−31).

For NEB, a new tool kit, which allows us to use arbitrary codes for the energies and forces calculations, was implemented. We use standard NEB with a force constant of ∼0.53 au (=1 HaÅ^{-1}) and the weighted tangent estimate described in ref 28. Since we expect MEP-s with several local minima and maxima, while it cannot be expected that the starting positions we choose for the surface adsorption of organic molecules from a gas phase correspond to local minima of the potential energy surface, we choose not to employ adaptive force constants as proposed in ref 32. For the same reason we also choose not to use climbing-image[33] NEB. We relax the NEB paths using a combination of projected velocity verlet and steepest descent methods, since our experience shows that the latter gives more rapid convergence at the beginning of the relaxation, while the former shows better behavior when the forces and curvatures are small. We employ the cubic polynomial fitting procedure described in the appendix of ref 28 to determine the energy profile of the MEP.

For the energy profiles along the MEP, we define a reaction coordinate x as the normalized total displacement along the direction $\hat{d}$ from the starting geometry $\vec{r}_{start}$ to the end geometry $\vec{r}_{end}$:

$$\hat{d} = \frac{\vec{r}_{end} - \vec{r}_{start}}{|\vec{r}_{end} - \vec{r}_{start}|} \tag{5}$$

$$x = \frac{1}{|\vec{r}_{end} - \vec{r}_{start}|}\sqrt{\vec{r}_i \cdot \hat{d}} \tag{6}$$

III. Model Preparation

A. Bulk γ-Al_2O_3. As stated in section I, the structure of γ-alumina is still under discussion in the literature. The consensus is, however, that it resembles a close packed oxygen (fcc) lattice with Al atoms and vacancies statistically distributed among the tetrahedral and octahedral sites. It can be generated either from a strained hausmannite or a spinel structure, by removing Al atoms to achieve Al_2O_3 stoichiometry. Due to the statistical distribution of vacancies, the structure can be regarded as *pseudoamorphous*.

We construct five different models of γ-Al_2O_3, one based on a hausmannite cell, one based on a rhombohedral representation of the spinel structure, and three based on a cubic representation of the spinel structure. For the cubic spinel case, we examine three different starting structures in which different Al atoms have been randomly removed. We relax the atomic positions in all cells, optimizing the cell volume. Table 2 lists the characteristic data of the relaxed cells. We find that the differences in terms of density of the optimized unit cell and Al−O bond lengths are negligible and that the densities correspond well to the experimentally reported value of 3.67 g cm^{-3}.[34] The energy differences between the three different basic structures (i.e., hausmannite, cubic spinel, and rhombohedral spinel) differ slightly indicating that the cubic representation is slightly favorable. Notably, the differences between the three different cubic spinel based models are negligible in all respects.

B. The Hydroxylated γ-Al_2O_3 Surface. To generate a model of the γ-Al_2O_3 surface, we choose the first of our 4-oxygen-layer thick, 160-atom cubic-spinel based models described above. We cut the bulk alumina by increasing the length of the cell vector along the (001) direction to 60 Å without changing any of the atomic positions. We then relax the resulting slab model using conjugate gradients (CG).

We hydroxylate this surface by placing a 10 Å thick layer of H_2O molecules, cut from a larger, geometry-optimized supercell of liquid water, on top of the surface model and then performing a 1 ps molecular dynamics (MD) run at 300 K, followed by a second 1 ps MD run at 600 K to remove the nonadsorbed water molecules. This procedure does not lead to chemisorption of water molecules at the surface, but since sufficiently long MD runs to achieve this are computationally far too expensive, we then manually split the water molecules, forming an OH group at the adsorption site and using the split-off hydrogens to protonate nearby Al−O−Al bridges. After this procedure, we

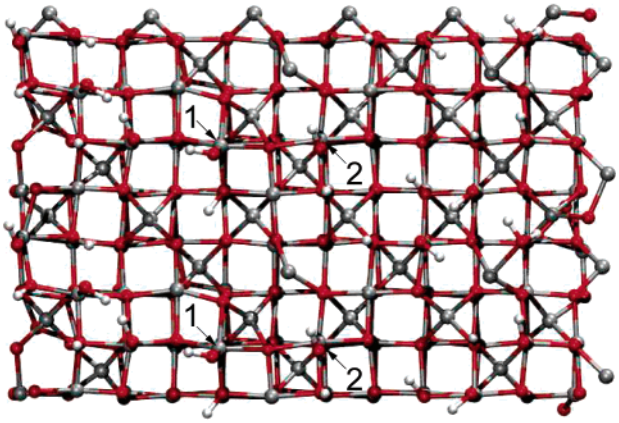

Figure 2. Plane view along the (001) direction of the hydroxylated γ-Al_2O_3 surface model (Al: gray; O: red; H: white). The selected adsorption sites are marked "1" and "2". (Note that, due to the periodic repetition, each adsorption site appears twice.)

relax the geometry using CG. During the whole procedure, the lowermost oxygen and aluminum layer was held fixed.

The surface supercell we generated this way has a surface area of $\sim 24 \times 8$ Å^2, which is too small in the (0, 1, 0) direction, therefore the surface model is duplicated along this axis. The resulting model contains 374 atoms in a $23.7 \times 15.8 \times 60$ Å^3 periodic supercell and is shown in Figure 2.

C. Adsorbed Molecules. After the surface model preparation, we select two different sites on the model, based on their different surroundings in terms of OH group density and density of underlying tetrahedrally coordinated Al atoms (cf. Figure 2). These sites will subsequently be referred to as site 1 and site 2. Two of the nearest neighbor Al-atoms of site 1 are not hydroxylated, three of site 2's nearest neighbor aluminums have no OH groups attached. Additionally, site 1 is in the vicinity of a cavity-like surface-Al vacancy, while one of the non-hydroxylated Al-neighbors of site 2 is atypically 2-fold coordinated. All reactions will be examined at these two sites. This will provide at least limited insight into the influence of the surface surroundings. While there are 13 possible inequivalent adsorption sites, we limit ourselves to these two sites for reasons of computational efficiency.

Next we prepare the models of our adsorbates by placing a relaxed model of the organic compound at the respective adsorption site, removing the OH group from the surface and one proton from the adhesive compound model and forming one C−O−Al, N−O−Al, or Si−O−Al bridge, respectively, following eqs 1−3. The resulting geometries are then relaxed with CG. We always include only one covalent bond between the organic compound and the surface in our input structures.

IV. Results

A. Reaction Energies. Figures 3−5 show the relaxed structures of the adsorbed organic compounds. The reaction energies calculated from the total energies of these structures and the total energies of the isolated compounds and isolated H_2O are listed in Table 2. It is noteworthy that the adsorption of DETA is pronouncedly endothermic. This observation can also be transferred to the amine-group of AMEO. The adsorption of t-DGEBA shows a strong dependence on the reaction site, so that the adsorption is significantly exothermic only at site 2. This corresponds to the observation that DGEBA forms a second bond to the surface at site 2 but not at site 1 (cf. Figure 3). AMEO displays the strongest exothermic behavior and only very little site-dependence—note that two surface bonds are formed at both

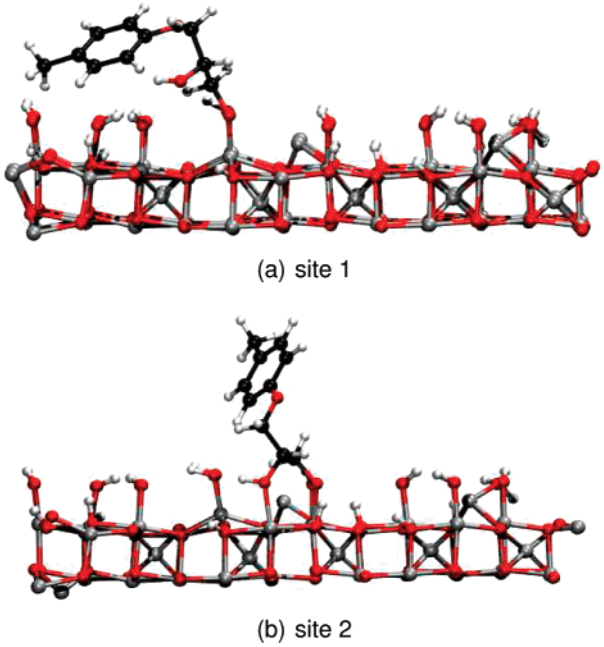

Figure 3. Structure of t-DGEBA adsorbed on the surface (Al: gray; O: red; H: white; the surface models are truncated in the (001) direction). Note that at site 2 an additional C−O−Al bridge to the surface was formed (cf. section IV.A).

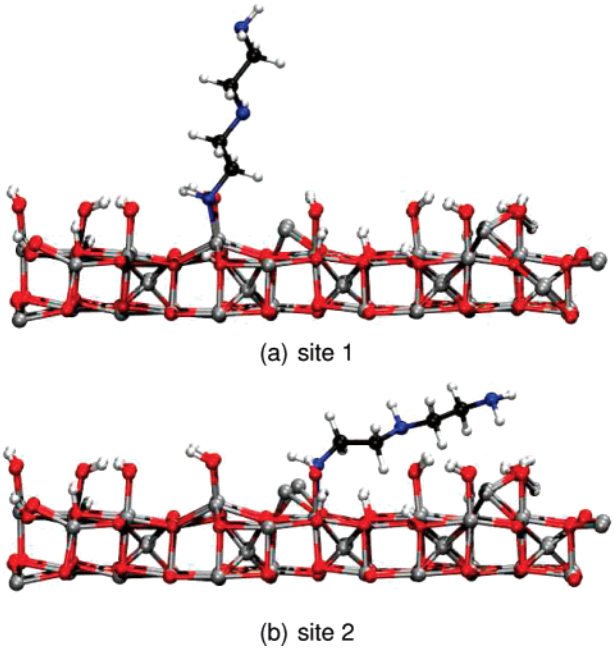

Figure 4. Structure of DETA adsorbed on the surface (Al: gray; O: red; H: white; N: blue; the surface models are truncated in the (00$\bar{1}$) direction).

reaction sites, as shown in Figure 5. At site 2, t-DGEBA forms a second C−O−Al bridge to the surface with bond lengths of 1.48 Å (C−O) and 1.94 Å (O−Al). The condensation of $AMEO^{hyd}$ leads to one additional Si−O−Al bridge with bond lengths of 1.70 ± 1 (Si−O) and 1.90 ± 1Å (O−Al) at both sites.

B. MEP-s. Table 2 lists the results of our MEP calculations. The root mean squares (RMS) of the forces perpendicular to the path direction are a measure of how well the chain of images lies in the valley of the potential energy surface; all paths appear well converged in that respect (cf. Table 2).

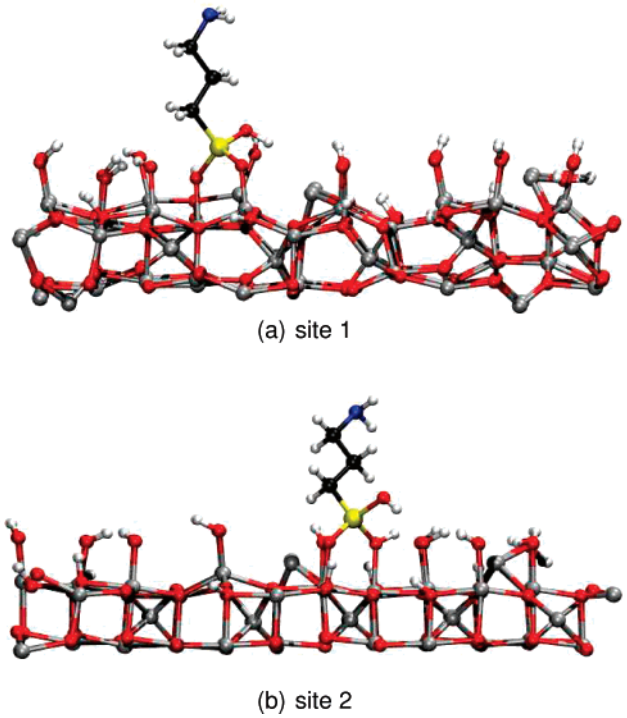

Figure 5. Structure of AMEO$^{(hyd)}$ adsorbed on the surface (Al: gray; O: red; H: white; N: blue; Si: yellow; the surface models are truncated in the (001) direction). Note that at both sites an additional Si−O−Al bridge to the surface was formed (cf. section IV.A).

TABLE 2: Reaction Barriers of the NEB Reaction Paths[a]

adsorbate	eq	site	barrier [kcal mol^{-1}]	reaction energy [kcal mol^{-1}]	$f^{\perp}_{RMS}$ [au]
t-DGEBA	1	1	82	−2.5	2.0×10^{-4}
	1	2	3	−36.9	2.0×10^{-4}
(ring opening)	4		50	−32.5	6.9×10^{-4}
DETA	2	1	28	+46.6	1.4×10^{-4}
	2	2	24	+54.3	1.0×10^{-4}
AMEO$^{(hyd)}$	3	1	< 1	−46.8	1.8×10^{-4}
	3	2	9	−44.9	1.3×10^{-4}

[a] Energies in kcal/mol, forces in H/Bohr.

The first reaction path we examine is the path of the ring-opening reaction of t-DGEBA catalyzed by water (eq 4). From the polynomial energy interpolation fitted to the image energies, we obtain a barrier energy of 49.8 kcal mol^{-1}. The trajectory of the image energies along the relaxation shows that, while the maximum NEB force per atom lowered from 2×10^{-3} to 10^{-4} au, the noninterpolated barrier energy changed by less than 0.1 kcal mol^{-1}. We therefore decide to choose our maximum force convergence criterion for the surface adsorption paths to 2×10^{-3} au. We also regard our calculations as converged, if the RMS of atomic NEB forces is below 2×10^{-4} au. Figure 6b shows the configuration closest to the transition state; the interpolated energy profile is shown in Figure 7.

For the condensation of t-DGEBA$^{(open)}$, the calculated MEP-s show a strong site-dependence of the barriers for the adsorption (cf. Figure 8). While at site 1 a pronounced barrier of about 80 kcal mol^{-1} appears (cf. Figure 9, the adsorption occurs nearly without barrier at site 2 (cf. Figure 10). At both sites, a difference between the reaction energies calculated from isolated educts and products and those obtained from the path of about 20 kcal mol^{-1} is observed. The additional energy gain in the path calculations comes from the physisorption of the water molecules, arising from the condensation reaction, to empty sites on the surface. [Relaxing a single water molecule, placed at the hydroxylated surface at the same location, where we find it after the condensation of t-DGEBA$^{(open)}$ at site 1, results in the formation of a surface−water complex, which yields 50 kcal mol^{-1} with reference to the isolated surface and water molecule.] This phenomenon cannot be avoided in the path calculations, since particle-number conservation must be observed and the water molecule cannot be removed from the surface without

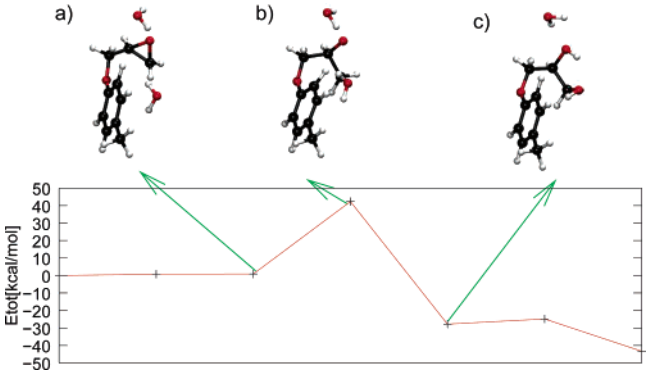

Figure 6. NEB path of the ring opening of t-DGEBA: the + symbols show calculated energies and the red line serves to guide the eye (C: black; O: red; H: white).

Ⓦ An animated.xyz file containing the reaction images is available.

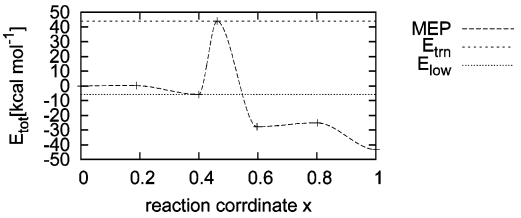

Figure 7. Interpolated energy profile of the ring opening of t-DGEBA by H_2O catalyzed by water. Zero energy is the total energy of the first image, reaction coordinate from eq 6.

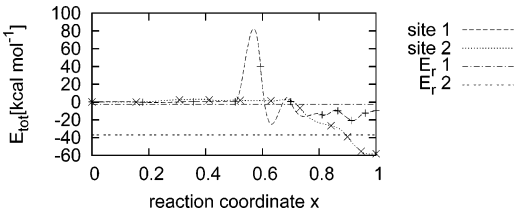

Figure 8. Interpolated energy profiles of the MEP-s and vacuum reaction energies of the condensation of t-DGEBA$^{(open)}$. Zero energy is the sum of the total energies of the isolated educts, reaction coordinate from eq 6.

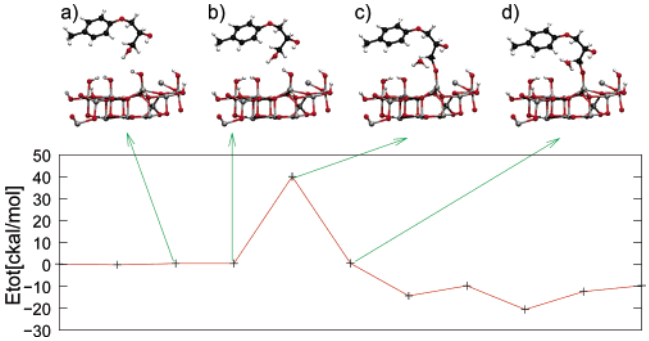

Figure 9. MEP of the adsorption of t-DGEBA$^{(open)}$ at site 1: the + symbols show calculated energies and the red line serves to guide the eye. The insets show a cutout of the surface surrounding the reaction site (C: black; O: red; H: white; Al: gray).

Ⓦ An animated.xyz file containing the start and end structures, as well as the shown intermediates, is available.

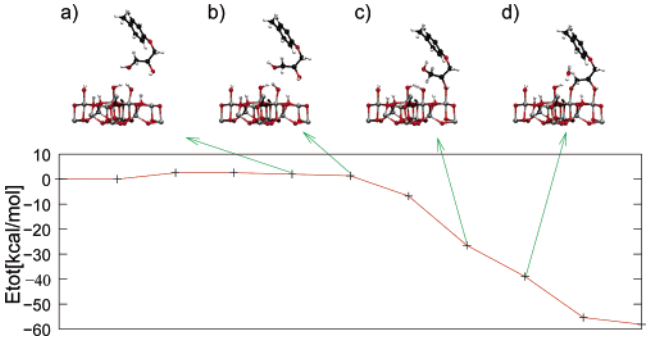

Figure 10. MEP of the adsorption of t-DGEBA$^{(open)}$ at site 2: the + symbols show calculated energies and the red line serves to guide the eye. The insets show a cutout of the surface surrounding the reaction site (C: black; O: red; H: white; Al: gray).

Ⓦ An animated.xyz file containing the start and end structures, as well as the shown intermediates, is available.

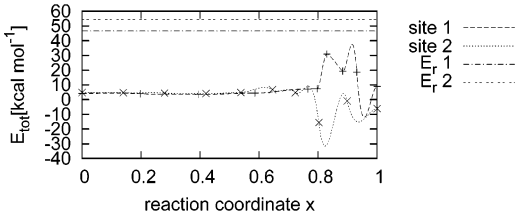

Figure 11. Interpolated energy profiles of the MEP-s and vacuum reaction energies of the condensation of DETA. Zero energy is the sum of the total energies of the isolated educts, reaction coordinate from eq 6.

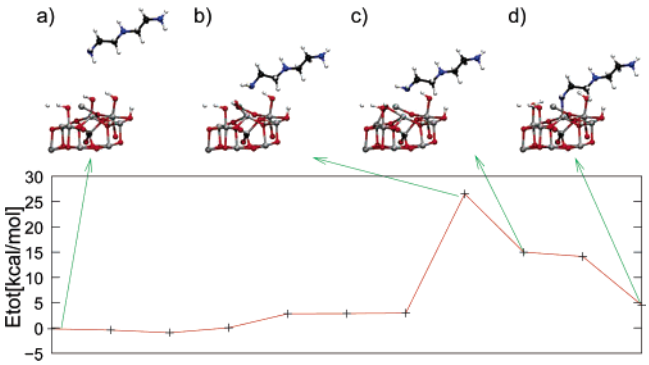

Figure 12. MEP of the adsorption of DETA at site 1: the + symbols show calculated energiesand the red line serves to guide the eye. The insets show a cutout of the surface surrounding the reaction site (C: black; O: red; H: white; N: blue, Al: gray).

Ⓦ An animated.xyz file containing the start and end structures, as well as the shown intermediates, is available.

introducing unphysical effects. Here, as in all reactions examined in this article, the energy gain from the water adsorption does not significantly influence the barrier energy, since the barrier occurs before the formation of the subsequently adsorbed water molecule. The lower reaction barrier at site 2 coincides with the formation of a second covalent bond to the surface.

Figure 11 shows the energy profiles of the DETA adsorption at both reaction sites. At both sites, the reaction depends on the dehydroxylation of a surface aluminum atom, as shown for site 1 in Figure 12, which is unfavorable and accounts for most of the reaction energy. As with the reaction of t-DGEBA$^{(open)}$, the generated water molecule is physisorbed at the surface, leading to a shift of the reaction energies of ~50 kcal mol^{-1} with respect to the results in Table 2. The reaction mechanism is the same at both site; the difference in reaction energies stems from a lower coulomb repulsion of the DETA molecule at site 2

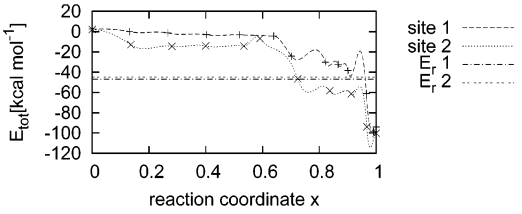

Figure 13. Energy profiles of the MEP-s and vacuum reaction energies of the condensation of AMEO^{hyd}. Zero energy is the sum of the total energies of the isolated educts, reaction coordinate from eq 6.

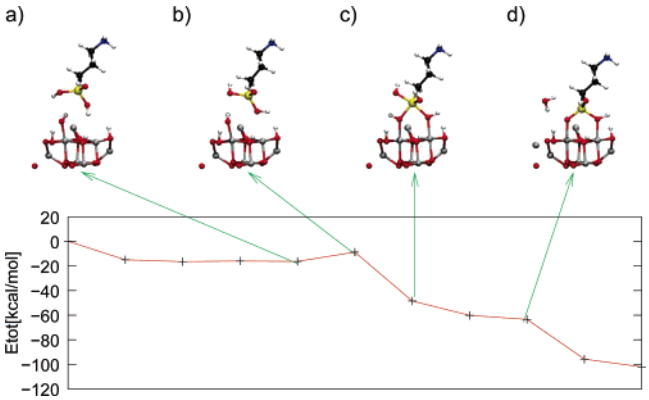

Figure 14. MEP of the condensation of AMEO$^{(hyd)}$ at site 2: the + symbols show calculated energies and the red line serves to guide the eye. The insets show a cutout of the surface surrounding the reaction site (C: black; O: red; H: white; N: blue; Al: gray; Si: yellow).

Ⓦ An animated.xyz file containing the start and end structures, as well as the shown intermediates, is available.

compared to site 1. At the former, the DETA molecule falls into a nonbonded, local minimum before the condensation reaction. The barrier for moving the surface OH group is listed as the reaction barrier for both sites in Table 2.

As can be seen in Figure 13 the MEP-s of the condensation of AMEO^{hyd} are very similar at both sites. In both cases, the barrier corresponds to a configuration in which the OH groups of the hydroxylated AMEO are coulomb repelled by the surface OH group, as shown in Figure 14b. A slight site dependence of this barrier is detected, but both detected barriers are negligible. With the formation of a covalent bond from the surface OH to the Si atom, resulting in a 5-fold coordination of the latter (cf. Figure 14c), the main energy gain is achieved. The subsequent H_2O formation from one of the AMEO^{hyd}'s OH groups and the H from the surface OH group is of lesser energetic impact. Again, the physisorption of the released water molecule releases about 50 kcal mol^{-1} compared to the reaction energy calculated from isolated products.

C. Influenced Surface Areas. The influence of the organic compound adsorption on the atoms of the Al_2O_3 surface was examined for the calculated MEP-s. Since the results are very similar for all examined reactions, we present, as an example, those obtained for AMEO$^{(hyd)}$ at site 2.

To determine the influence of the adsorption reaction on the surface geometry, the RMS of the displacement (RMSD) of each atom along the path, with reference to the starting geometry, was calculated. It is shown color-coded in Figure 15. It can be clearly seen that most atoms move by less than 0.05 Å. Outside a radius of ~5 Å in the surface plane and below the second oxygen layer from the surface, no surface atoms move significantly, while the surface OH groups show some reorientation.

Similar to the atom displacements, we examine the electronic influence of the adsorption reaction. We calculate the difference

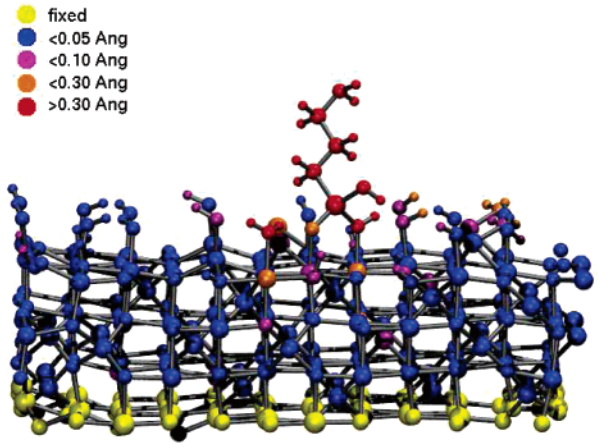

Figure 15. Movement of the atoms during the adsorption of AMEO$^{(hyd)}$ at site 2: color coded by RMSD over the entire reaction path.

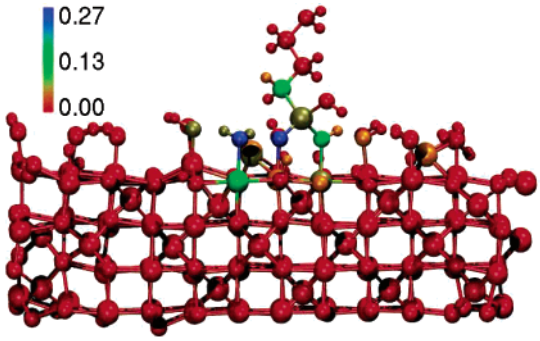

Figure 16. Mulliken charge difference $\Delta Q = Q_{max} - Q_{min}$ during the reaction of AMEO$^{(hyd)}$ at site 2, color-coded for each atom in units of e^-.

of the maximum and minimum Mulliken charges along the path for each atom. The results are shown color-coded in Figure 16. It can be seen that the charge transfers are very small. The range of electronic influence is slightly larger than that of the mechanical influence but still small. Charge transfers of ~0.1 e^- can be seen at the reoriented surface OH groups.

V. Discussion

The comparison of the calculated reaction energies listed in Table 2 shows that the condensation of DETA is extremely unfavorable with regard to the other examined components. The endothermicity of ~50 kcal mol^{-1} makes these reactions very unlikely.

The results concerning the condensation reactions of AMEO$^{(hyd)}$ and t-DGEBA$^{(open)}$ are more differentiated. At site 2, both reactions show roughly the same exothermic behavior with a difference in reaction energies on the order of 10 kcal mol^{-1}, from which, considering the approximations employed, no clear preference for one reaction or the other can be established. In contrast, at site 1 condensation of t-DGEBA$^{(open)}$ yields only a negligible amount of energy, while AMEO$^{(hyd)}$ shows the same exothermicity as at site 2.

From these observations, it can be concluded that DGEBA will not be able to bond to all surface OH groups, thus, on one hand, limiting the maximum adhesive force that can be created from DGEBA bonding to the surface. On the other hand, the lower density of potential binding sites, induced by the site dependence of reaction energies and barriers, limits the probability that DGEBA molecules will bind to the surface with both its epoxy groups, which is unwanted since it occupies adsorption sites without leading to interconnection between surface and polymer. This would lead to the formation of a DGEBA monolayer with only weak bonding to the bulk polymer, which would be a natural breaking point for an adhesive joint.

We find no evidence for site-dependent effects on the adsorption of AMEO^{hyd}. This leads to the conclusion that the surface coverage with AMEO is limited by the density of surface OH groups. This, at least partly, explains the adhesion promoting effect of AMEO. We have shown that it can form strong bonds to the surface at sites to which DGEBA can only weakly bind. This allows the number of covalent bonds between the surface and the bulk polymer to increase. Additionally, the amine group of AMEO is very unlikely to bind to the surface, as the reaction mechanism is essentially the same as that of the amine groups of DETA. Thus the formation of an AMEO layer between surface and bulk polymer that is only weakly bound to one side will not occur.

The reaction barriers listed in Table 2 do not qualitatively change the picture derived from the reaction energies but support the conclusions drawn above. The barriers for the condensation of AMEO^{hyd} are small enough to be considered negligible. The same holds for the condensation of t-DGEBA$^{(open)}$ at site 2, where the adsorption is energetically favorable. The low energy gain from the adsorption of t-DGEBA$^{(open)}$ at site 1 is accompanied by a high reaction barrier. From the differences in reaction barriers it becomes clear that at site 1 the condensation of AMEO$^{(hyd)}$ is highly favored while at site 2 both reactions are competitive, while the reaction energies hint that the condensation of AMEO$^{(hyd)}$ may be slightly favorable. It should be noted that the condensation of t-DGEBA at site 1 is the only reaction for which we find a significant barrier caused by the water formation. It can be expected that the presence of solvent water in the vicinity of this reaction will lower this barrier, by stabilizing the transition state.

Concerning DETA, our results show that the examined adsorption mechanism depends on the highly unfavorable dehydoxylation of surface aluminum atoms. A future study of the barriers for the chemisorption of DETA at nonhydroxylated surface aluminum atoms would be of interest to examine other possible adsorption mechanisms.

It should be pointed out that, as we examined only adsorption from the gas phase, our results alone are only one step toward an atomistic understanding of the influence of the particular component's on the properties on the adhesion behavior of an adhesive mixture. Important effects, such as the (partial) desolvation of the molecules from the adhesive mixture, which is prerequisite to the adsorption of a molecule from any adhesive liquid applied to the surface, are not reflected in these model calculations. Also, effects connected to the (pre-)polymerization of the adhesive mixture before, during, and after the application to the surface, which may strongly influence the mobility of the component molecules and their ability to bind to the surface, are outside the scope of this study. Only in conjuction with considerations regarding these and other issues such as changes in the relative concentrations of the components in the adhesive mixture, which may be indiced by the surface adsorption, can a wider understanding of the bonding between the oxide surface and polymers be achieved.

Concerning reaction mechanisms of the examined condensation reactions, we find that all energetically favorable reactions involve neighboring surface aluminum atoms without OH groups. Especially the site dependence of t-DGEBA$^{(open)}$ suggests that the formation of a protonated Al−O bridge plays a crucial role in determining the reaction energetics. This mechanism is likely to be influenced by the presence of physisorbed

water at the surface. Thus it appears desirable to be able to examine solvent effects on the reactions regarded here. With the choice of methods employed here, the computational cost for the inclusion of a significant amount of water is prohibitive. Therefore the reactions examined here present themselves as a well-suited application for the development of multiscale methods which would allow the effects of a polar solvent with manageable computational effort to be included.

The calculated ranges in which the adsorption reactions influence the surface electronically and mechanically are limited to a range of ca. ±5 Å lateral and ~5 Å perpendicular to the surface. Both results were expected from a stiff dielectric material but had to be verified nonetheless. Our results lead to the conclusion that most of the large surface model, necessary to obtain the correct alumina stoichiometry and to avoid self-interaction of the adsorbate with its periodic images, need not be treated with quantum mechanical precision. It is, in principle, possible to define two separate parts of the surface, one of which can be simulated by using force fields, while the other must be treated quantum mechanically. This proves that the problem of the adhesion of organic molecules to alumina surfaces, as well as other hard, dielectric inorganic surfaces, is susceptible to multiscale approaches.

Additionally, the limited ranges of influence lead to conclusions concerning the methods and embedding scheme necessary for a multiscale modeling of these adhesions. The observation that the range of significant charge transfer is well defined on a scale of 5−10 Å shows that the inner zone requires a quantum mechanical method, efficient enough to describe 10−100 atoms with sufficient speed for the desired calculations, otherwise problems caused by the neglect of charge transfer across the zone border are to be expected. At the same time, the observation that the surface area, in which significant atom displacements are observed, is somewhat smaller than the QM zone necessary for the electronic influence indicates that the interatomic forces across the zone boundary will not be the predominant cross-boundary interaction. Therefore the electrostatic interaction between the zones, at least on the level of polarization of the QM zone from the MM zone, must be included in a multiscale coupling scheme to analyze organic molecule adhesion on stiff dielectric surfaces.

VI. Conclusion

We have shown that the condensation of the adhesion promoter $AMEO^{(hyd)}$ via its silane group is, in total, favorable over the adsorption of the other two examined adhesive components DGEBA and DETA. The condensation is significantly exothermic and has negligible barriers at both examined surface sites. The condensation of the curing agent component DETA, via its amine group, interacting with a surface hydroxyl group is pronouncedly endothermic, a result that can also be transferred to the amine group of AMEO. Energetically, the condensation of ring-opened DGEBA is only competitive at a subset of the available adsorption sites. Additionally, the condensation is dependent on the prior opening of an epoxy ring of the DGEBA molecule, which has a high barrier. The pronounced differences in reaction energies and barriers allow viable qualitative conclusions about the adsorption competition of different EP species on the γ-alumina surface, despite the methodological limitations we encountered. It has become clear that the amine curing agent will not significantly adsorb to OH groups at the alumina surface. The competition between DGEBA and similar epoxy resins and AMEO will be biased in favor of AMEO, since the former depends on a preliminary reaction in the adhesive mixture with a significant barrier and because the latter can condense at more surface sites with only negligible activation energies.

Although our results show clear trends for the different adhesive components, it becomes clear that further studies including solvent effects should be performed to improve the insight into adhesion behavior.

Our results concerning the influence areas suggest that it will be possible to model a large part of the surface using a fixed distribution of point charges or molecular mechanics. This will dramatically reduce the computational cost of total energy and gradient calculations. Together with the inclusion of a molecular-mechanical water model, this will allow us to include solvent effects into future calculations and might even allow for the calculation of free energies along the adsorption paths. Both steps are planned for future work.

Acknowledgment. Financial support from the DFG SPP-1155 is greatly appreciated. The authors thank the Paderborn Center for Parallel Computing, PC^2 for computing time on the ARMINIUS cluster. J.M.K. greatly appreciates the useful input from Michael Hoffmann and Peter König in matters of reaction path search methods. J.M.K. is grateful to Bálint Aradi for fruitful discussions about PYTHON programming techniques. Molecular visualizations were prepared with vmd.[35]

References and Notes

(1) Straznicky, P. V.; Laliberté, J. F.; Poon, C.; Fahr, A. *Polym. Compos.* **2000**, *21*, 558−567.

(2) Wefers, K.; Misra, C. Oxides and Hydroxides of Aluminum, Technical Report, Alcoa Laboratories, 1987.

(3) Holleman, A. F.; Wiberg, E. Das Aluminium. In *Lehrbuch der Anorganischen Chemie*; Wiberg, N., Ed.; de Gruyter: Berlin, Germany, 1995; pp 1081−1083.

(4) Lee, M.-H.; Cheng, C.-F.; Heine, V.; Klinowski, J. *Chem. Phys. Lett.* **1997**, *265*, 673−676.

(5) Wolverton, C.; Hass, K. C. *Phys. Rev. B* **2000**, *63*, 024102.

(6) Saalfeld, H.; Mehrotra, B. *Ber. Dtsch. Keram. Ges.* **1965**, *42*, 161−166.

(7) Chou, T. C.; Nieh, T. G. *J. Am. Ceram. Soc.* **1991**, *74*, 2270.

(8) Lippens, B. C.; de Boer, J. H. *Acta Crystallogr.* **1964**, *17*, 1312−1321.

(9) Maresca, O.; Ionescu, A.; Allouche, A.; Aycard, J.; Rajzmann, M.; Hutschka, F. *J. Mol. Struct.-Theochem* **2003**, *620*, 119−128.

(10) Paglia, G.; Rohl, A. L.; Buckley, C. E.; Gale, J. D. *Phys. Rev. B* **2005**, *71*, 224115.

(11) Paglia, G.; Buckley, C. E.; Rohl, A. L.; Hunter, B. A.; Hart, R. D.; Hanna, J. V.; Burne, L. T. *Phys. Rev. B* **2003**, *68*, 144110.

(12) G. Paglia, G. Determination of the Structure of γ-Alumina using Empirical and First Principles Calculations combined with Supporting Experiments, Thesis, Curtin University of Technology, Perth, 2004.

(13) Peri, J. B. *J. Phys. Chem.* **1965**, *69*, 220−230.

(14) Peri, J. B. *J. Phys. Chem.* **1965**, *69*, 211−219.

(15) De Boer, J. H.; Fortuin, J. M.; Lippens, B. C.; Meijs, W. H. *J. Catal.* **1963**, *2*, 1−7.

(16) Maciver, D. S.; Tobin, H. H.; Barth, R. T. *J. Catal.* **1963**, *2*, 485−497.

(17) Maresca, O.; Allouche, A.; Aycard, J. P.; Rajzmann, M.; Clemendot, S.; Hutschka, F. *J. Mol. Struct.-Theochem* **2000**, *505*, 81−94.

(18) De Vito, D. A.; Gilardoni, F.; Kiwi-Minsker, L.; Morgantini, P.-Y.; Porchet, S.; Renken, A.; Jacques Weber, J. *J. Mol. Struct.-Theochem* **1999**, *469*, 7−14.

(19) Movarek, V.; Kraus, M.; Malysheva, L. V.; Paukshtis, E. A.; Yurchenko, E. N. *Czech Chem. Commun.* **1988**, *53*, 459.

(20) Schneider, B.; Hennemann, O.-D.; Possart, W. *J. Adhes.* **2002**, *78*, 779−797.

(21) Krüger, T.; Amkreutz, M.; Schiffels, P.; Schneider, B.; Hennemann, O.-D.; Frauenheim, T. *J. Phys. Chem. B* **2005**, *109*, 5060−5066.

(22) Schneider, B.; Schiffels, P.; Wilken, R. Bonding Of Amine Cruing Agents To Native Aluminum Oxide Surfaces. In *Proceedings of the 28th Annual Meeting of the Adhesion Society*; February 13−16, 2005, Mobile, Alabama; 2005.

(23) Frauenheim, T.; Seifert, G.; Elstner, M.; Hajnal, Z.; Jungnickel, G.; Porezag, D.; Suhai, S.; Scholz, R. *Phys. Status Solidi B* **2000**, *217*, 41.

(24) Krüger, T.; Elstner, M.; Schiffels, P.; Frauenheim, T. *J. Chem. Phys.* **2005**, *122*, 114110.
(25) Soler, J. M.; Artacho, E.; Gale, J. D.; Garcia, A.; Junquera, J.; Ordejón, P.; Sanchéz-Portal, D. *J. Phys.*: *Condens. Matter* **2002**, *14*, 2745.
(26) Troullier, N.; Martins, J. L. *Phys. Rev. B* **1991**, *43*, 1996.
(27) Jónsson, H.; Mills, G.; Jacobsen, K. W. Nudged elastic band method for finding minimum energy paths of transitions. In *Classical and Quantum Dynamics in Condensed Phase Simulations*; Berne, B. J., Ciccotti, G., Coker, D. F., Eds.; World Scientific: Singapore, 1998; pp 387−405.
(28) Henkelman, G.; Jónsson, H. *J. Chem. Phys.* **2000**, *113*, 9978−9985.
(29) Du, A. J.; Smith, S. C.; Yao, X. D.; Lu, G. Q. *J. Phys. Chem. B* **2005**, *109*, 18037−18041.
(30) Sbraccia, C.; Pignedoli, C. A.; Catellani, A.; Di Felice, R.; Silverstrelli, P. L.; Toigo, F.; Ancilotto, F.; Bertoni, C. M. *Comput. Phys. Commun.* **2005**, *169*, 32−35.
(31) Bakos, T.; Valipa, M.; Aydil, E. S.; Maoudas, D. *Chem. Phys. Lett.* **2005**, *414*, 61−65.
(32) Maragakis, P.; Adreev, S. A.; Brumer, Y.; Reichmann, D. R.; Kaxiras, E. *J. Chem. Phys.* **2002**, *117*, 4651−4658.
(33) Henkelman, G.; Uberuaga, B. P.; Jónsson, H. *J. Chem. Phys.* **2000**, *113*, 9901−9904.
(34) Wyckoff, R. W. G. *Crystal Structures*; Interscience: New York, 1965.
(35) Humphrey, W.; Dalke, A.; Schulten, K. *J. Mol. Graph.* **1996**, *14*, 33−38.